Appl Nanosci (2015) 5:481–491
DOI 10.1007/s13204-014-0340-3

ORIGINAL ARTICLE

Preparation and electrochemical characterization of manganese dioxide-zirconia nanorods

R. R. Muthuchudarkodi · C. Vedhi

Received: 20 May 2014 / Accepted: 10 July 2014 / Published online: 3 August 2014

Abstract MnO_2–ZrO_2 nanorods were prepared by wet chemical method by mixing the solutions of $MnSO_4$ and $ZrOCl_2$ varying in the range (0.05–0.45 M) in aqueous NaOH at an elevated temperature. The morphologies of the synthesized products are characterized by scanning electron microscopy and transmission electron microscopy (TEM). X-ray diffraction (XRD) and energy-dispersive spectroscopic measurements were also employed for the characterization of the nanostructures. The synthesized nanoparticles were also characterized by ultraviolet visible spectroscopy, Fourier transform infrared spectroscopy, electrochemical impedance and cyclic voltammetric studies. The morphological studies of the nanoparticles revealed particle distribution with uniform rod-like structure. Energy-dispersive analysis indicated the presence of Mn, Zr and O. The nanostructures of the product were characterized by TEM studies and the mixed rod and granular structure that was found clearly indicated the presence of MnO_2–ZrO_2 mixed oxide. The size of the synthesized nanorod was found to be 20 nm. From XRD studies the size of the nanorods was found to be in the range 39–56 nm calculated by Debye–Scherrer's formula. Thermal stability of the nanorods was characterized by thermogravimetric and differential scanning colorimetric analysis. Cyclic voltammetric studies exhibit good adherent behavior on electrode surface and good electroactivity at a pH value of 1.0.

Keywords MnO_2–ZrO_2 nanorods · Impedance · SEM · TEM and cyclic voltammetry

R. R. Muthuchudarkodi · C. Vedhi (✉)
Department of Chemistry, V.O Chidambaram College, Tuticorin 628008, Tamilnadu, India
e-mail: cvedhi23@gmail.com; cvedhi@rediffmail.com

R. R. Muthuchudarkodi
e-mail: muthu.rajaram@gmail.com

Introduction

One-dimensional (1D) nanostructured materials, including nanotubes, nanorods, and nanowires, have attracted intense research interest, owing to their novel physical and chemical properties (Chen et al. 2005). Various methods have been developed to prepare various 1D nanomaterials, such as arc discharge, laser ablation, chemical vapor deposition, templating, and hydrothermal methods, etc. MnO_2 is one of the most attractive materials due to its ion exchange, molecular adsorption, catalytic, electrochemical, and magnetic properties (Chen et al. 2005). They are widely used as catalysts (Chen et al. 2005; Brock et al. 1998; Shi et al. 2010) molecular-sieves, ion-sieves (Feng et al. 1999) and especially as electrode materials in Li/MnO_2 batteries because of its energetic compatibility in a reversible lithium electrochemical system, eco-friendliness, and low cost. The properties of MnO_2 depend not only on the manganese oxidation state, but also on the structure type of MnO_2 crystal. Great effort has been made to prepare nanocrystalline MnO_2 with different structures. Over the past few years, the synthesis of nanostructures with controllable size and shape has been increased attracting attention (Dong et al. 2006). Manganese compounds, such as various manganese oxides/oxyhydroxides have been noticed owing to their specialities. Manganese oxyhydroxides, MnOOH, are of considerable importance in many technological applications, e.g., electrochemical reaction, battery and electrochromic application (Dong et al. 2006). Mn_3O_4 is known to be an active catalyst in several oxidations and reductions, and can be used as a catalyst for the oxidation of methane and carbon monoxide of the selective reduction of nitrobenzene (Dong et al. 2006). Nanorods have potential applications in nanodevices (Xia et al. 2003; Lu and Lieber 2006). Manganese

oxides have a wide range of applications such as battery materials (Hosono et al. 2009), catalysts and sensors. At present, a tremendous amount of comprehensive investigations are under way into the unique applications of nanorods and nanotubes, because they provide a great opportunity to investigate the dependence of optical/electrical properties, thermal transport, and mechanical performance on the nano-scaled dimensionality and size (Wang 2000). Nanomaterials, especially nanorods have enhanced performances in many fields such as sensors (Dietl et al. 2000), solar cells (Yu 2009) catalysts and battery materials. Of the various non-noble metals or transition-metal oxides studied, MnO_2 enjoys a place of pride because of its cost-effectiveness and eco-friendly nature. Beyond these advantageous properties, MnO_2 is a very promising material in a neutral electrolyte system. In the case of pseudo capacitors, various noble and transition-metal oxides such as RuO_2, IrO_2, NiO, CoOx, SnO_2 and MnO_2 were used as electrode materials (Subramanian et al. 2008). Zirconium dioxide is the most studied ceramic material. Pure ZrO_2 has a monoclinic structure at room temperature and transitions to tetragonal and cubic at increasing temperature. Zirconia supports are of particular interest as they can possess relatively high surface areas; they are mechanically and thermally stable and are solids with adsorbent properties, as well as catalysts themselves. Wambach et al. (1999) have recently reviewed the preparation of metal–zirconia catalysts along with their structural and chemical characteristics. Stabilized zirconia is used in oxygen sensors, fuel cell membranes and electroceramics. It will be used as insulators in transistors in future nanoelectronic devices. In this study an attempt has been made to synthesize and characterize novel, mixed MnO_2–ZrO_2 nanorods.

Experiment

Materials

The precursors zirconiumoxychloride ($ZrOCl_2$), manganese sulfate ($MnSO_4$) and the precipitant (NaOH) were purchased from Aldrich. All solutions were made up with deionised water.

Preparation of simple metal oxide nanoparticles

Fifty milliliters of 0.1 M $MnSO_4$ was added dropwise to an aqueous solution of NaOH (50 ml, 1.0 M), making a final volume of 100 ml. The mixture was stirred well and refluxed at an elevated temperature for 2.0 h. The sample was collected by centrifugation, washed with water and dried over for 4 days at room temperature. Similar procedure was carried out for the preparation of ZrO_2 nanoparticles using $ZrOCl_2$ as the precursor.

Preparation of MnO_2–ZrO_2 nanorods

MnO_2–ZrO_2 nanorod was prepared by wet chemical method. In this method, 25 ml of 0.45 M $ZrOCl_2$ was added to the aqueous solution of 50 ml of 1.0 M NaOH solution and stirred well. To this mixture, 25 ml of 0.45 M $MnSO_4$ was added making a final volume of 100 ml. The resulting mixture was stirred well and refluxed at an elevated temperature for 2.0 h. The sample was collected by centrifugation, washed with water and dried over for 4 days at room temperature. Similar procedure was carried out to prepare different concentrations of (0.05–0.35 M) MnO_2–ZrO_2 mixed oxides.

Characterizations

The solution of the metal oxide nanoparticles in DMSO was used for recording the ultraviolet visible spectroscopic (UV–Vis) spectra. For recording the UV–Visible absorption spectra, a computer-controlled JascoV-500 spectrophotometer was used. The FTIR spectra were recorded using a Shimadzu instrument. The X-ray diffraction (XRD) patterns were recorded for the powdered materials using a Bruker AXS (D8 Advance) X-ray diffractometer. Energy-dispersive spectroscopic (EDAX) and SEM measurements were carried out by JEOL JSM-6360F field emission scanning electron microscope. Transmission electron microscopy (TEM) images were recorded using Philips CM 200 model with the operating voltage range 20–200 and with a resolution of 2.4 Å.

The electrochemical studies were carried out in a three-electrode cell. Pt wire was used as a counter electrode, silver–silver chloride electrode as a reference electrode and metal oxide nanoparticle-coated GCE was used as working electrode. The impedance studies were carried out using electrochemical workstation (mode 650C), CH-Instrument Inc., TX, USA. The charge transfer resistance was obtained from the diameter of the semicircles of the Nyquist plots. TGA/DTA analysis was carried out using PerkinElmer model and DSC analysis using METTLER TOLEDO model.

Result and discussion

UV–Vis studies

Ultraviolet visible (UV–Vis) absorbtion spectra of nano MnO_2, nano ZrO_2 and mixed MnO_2–ZrO_2 were recorded in the range 200–800 nm as shown in (Fig. 1). The absorption

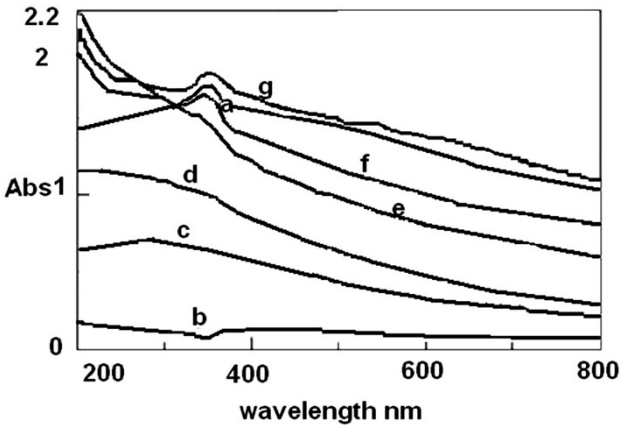

Fig. 1 UV-VIS spectra of (*a*) nano MnO_2, (*b*) nano ZrO_2, (*c*) 0.05 M MnO_2–ZrO_2, (*d*) 0.15 M MnO_2–ZrO_2, (*e*) 0.25 M MnO_2–ZrO_2, (*f*) 0.35 M MnO_2–ZrO_2, (*g*) 0.45 M MnO_2–ZrO_2

wavelength appears at 348 nm for nano MnO_2 (Luo et al. 2004) and 335 nm for nano ZrO_2. The absorption peaks for different concentrations (0.05–0.45 M) of MnO_2–ZrO_2 mixed oxides have been found to be in the range 281–348 nm, and are shown in Fig. 1. The variations in the absorption peaks for simple and mixed oxides are due to the smaller size of the nanoparticles (Singh et al. 2012). The mixed oxide nanoparticles exhibited blue shift compared with that of the simple oxides. The blue shift of the absorption peaks of the metal oxide nanoparticles result from certain unique effects of nanomaterials such as nanoscale effect and the blue shift reduces absorption of longer wavelength and is thus undesirable for UV protection (Yang et al. 2004). The absorption peaks of metal oxide nanoparticles appeared at a shorter wavelength region. Thus the metal oxide nanoparticles are found to be

Fig. 2 FTIR Spectra of (a) nano ZrO_2, b nano MnO_2, c 0.05 M MnO_2–ZrO_2, d 0.15 M MnO_2–ZrO_2, e 0.25 M MnO_2–ZrO_2, f 0.35 M MnO_2–ZrO_2, g 0.45 M MnO_2–ZrO_2

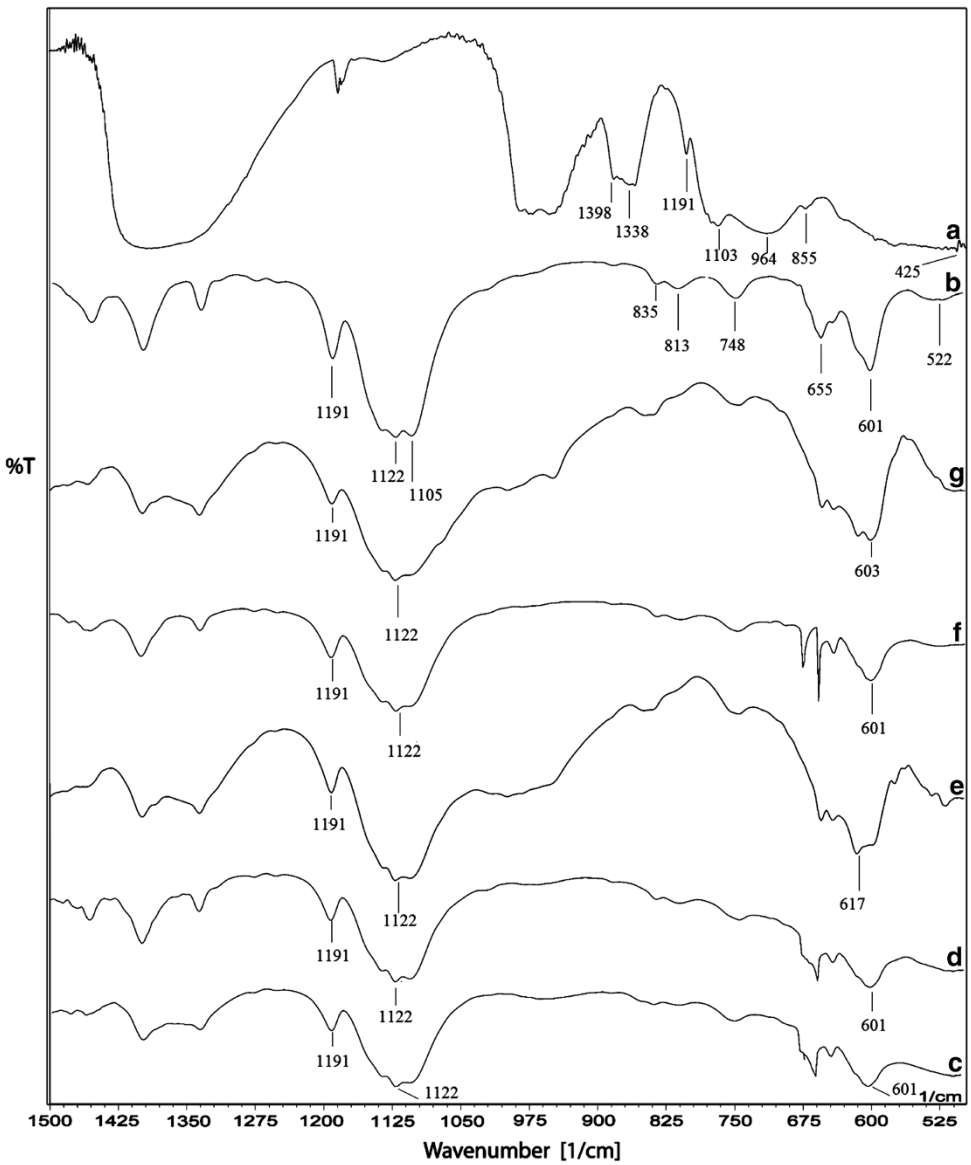

solar UV blockers (Yang et al. 2004). With the increase in concentrations of nano MnO_2–ZrO_2 mixed oxides there appeared increase in absorption values.

FTIR studies

Metal oxides generally give absorption bands below 1,000 cm^{-1} that arise from interatomic vibrations given in Fig. 2. The frequencies observed at 511–954 and 425–964 cm^{-1} correspond to Mn–O (Rema Devi et al. 2007) and Zr–O (Pérez-Maquedaa and Matijevicb 1997) bond vibrations, respectively. The peaks observed at 1,336 and 1,338 cm^{-1} are assigned to O_2 stretching frequency (Guedes et al. 2009). Symmetric frequencies of Mn–O and Zr–O were observed at 1,191 and 1,103 cm^{-1} (Guedes et al. 2009; Du et al. 2009). The peak observed at 3,401 cm^{-1} corresponds to O–H vibration of water. The characteristic peaks observed at 1,122 and 1,103 cm^{-1} are due to the presence of inorganic ions (Rema Devi et al. 2007).

Fourier transform infrared spectroscopic (FTIR) spectra of MnO_2–ZrO_2 mixed oxides synthesized at five different concentrations of both $MnSO_4$ and $ZrOCl_2$ (0.05, 0.15, 0.25, 0.35 and 0.45) are shown in Fig. 2c–g. For mixed oxide nanorods (0.45 M) MnO_2–ZrO_2, the combination of both Mn–O and Zr–O bonds appear in the range 511–999 cm^{-1} Fig. 2g. The frequencies observed at 1,336 and 1,396 cm^{-1} are assigned to O_2 stretching and bending frequencies, respectively (Partha Sarathi and Thilagavathi 2011). The characteristic peak at 1,122 cm^{-1} clearly indicates the presence of inorganic ions (Du et al. 2009). In the case of other concentrations of (0.05–0.35 M) MnO_2–ZrO_2 mixed oxides, the bands were almost similar to 0.45 M MnO_2–ZrO_2.

SEM and EDAX behaviors of nano MnO_2, nano ZrO_2 and MnO_2–ZrO_2

Scanning electron microscopy (SEM) was used to identify the morphology of the synthesized metal oxides and mixed metal oxides MnO_2, ZrO_2 and MnO_2–ZrO_2. From Fig. 3a, b the prepared MnO_2 and ZrO_2 display sponge-like structure, granular flakes and mixed granular appearance. When $MnSO_4$ and $ZrOCl_2$ were mixed, the surface morphologies and roughness of the particles are changed to rod-like structure and become homogeneous which confirmed the formation of MnO_2–ZrO_2 nanoparticles. SEM micrographs of nano MnO_2–ZrO_2 synthesized at five different concentrations of both $MnSO_4$ and $ZrOCl_2$ (0.05, 0.15, 0.25, 0.35, and 0.45) are shown in Fig. 3c–g. Particles synthesized in 0.05 M of $MnSO_4$ and $ZrOCl_2$ appear to be very uniform in spherical morphology. In the case of 0.15 M of $MnSO_4$ and $ZrOCl_2$ and 0.25 M of $MnSO_4$ and $ZrOCl_2$, the particles were modified from spherical into rod-like morphology. However, the nano MnO_2–ZrO_2 mixed oxides synthesized in the 0.35 M of $MnSO_4$ and $ZrOCl_2$; 0.45 M of $MnSO_4$ and $ZrOCl_2$ were completely changed into nanorods. By choosing the adequate concentration we would be able to form nanorods. EDAX analysis confirms the presence of Mn, Zr and O as shown in Fig. 3.

TEM behaviors of nano MnO_2, nano ZrO_2 and MnO_2–ZrO_2

Transmission electron microscopy (TEM)'s image of MnO_2 nanoparticles shows the size of the nanoparticles to be 20 nm and Fig. 4a shows the size of the ZrO_2 nanoparticles to be 100 nm. The morphology of the synthesized nano ZrO2 also appeared rod-like and that of nano MnO2, sphere-like (Fig. 4b). The morphology of mixed nano metal oxide (0.45 M of MnO_2–ZrO_2) was found to be a uniform rod and the size is observed to be 20 nm as shown in Fig. 4c.

XRD behaviors of nano MnO_2, nano ZrO_2 and MnO_2–ZrO_2

The X-ray powder diffraction patterns for the simple and mixed oxide nanoparticles as in Fig. 5 are typical of crystalline nanoparticles. The particle size was calculated using Scherrer's equation. In the case of nano MnO_2 the particle size was 45 nm and in the case of nano ZrO_2 the particle size was 8.3 nm. The average crystallite sizes of nanorods, MnO_2–ZrO_2 is found to be in the range of 39–56 nm. With the increase in concentrations of MnO_2–ZrO_2 from 0.05 to 0.45 M there is corresponding increase in size. The sharp peaks indicate more crystallinity and hence it shows more conductivity because high crystallinity materials usually show higher conductivity.

Thermal analysis

Figure 6 shows the thermograms of nano ZrO_2, nano MnO_2 and different concentrations of mixed MnO_2–ZrO_2 oxides. Figure 6a shows the TGA/DTA behavior of MnO_2. The first weight loss step from 42 to 90 °C corresponds to loss of moisture. The next step from 91 to 580 °C was due to the presence of extra bounded water molecules. The final weight loss step from 581 °C onwards corresponds to the degradation of MnO_2. The first weight loss step from 30 to 100 °C (Fig. 6b) corresponds to loss of moisture. The next step from 101 to 170 °C was due to the presence of extra bounded water molecules. The final weight loss step from 170 °C onwards corresponds to the degradation of ZrO_2. The DTA analysis also exhibited the same behavior.

Thermal stability of nano MnO_2–ZrO_2 mixed oxides synthesized at five different concentrations of both $MnSO_4$

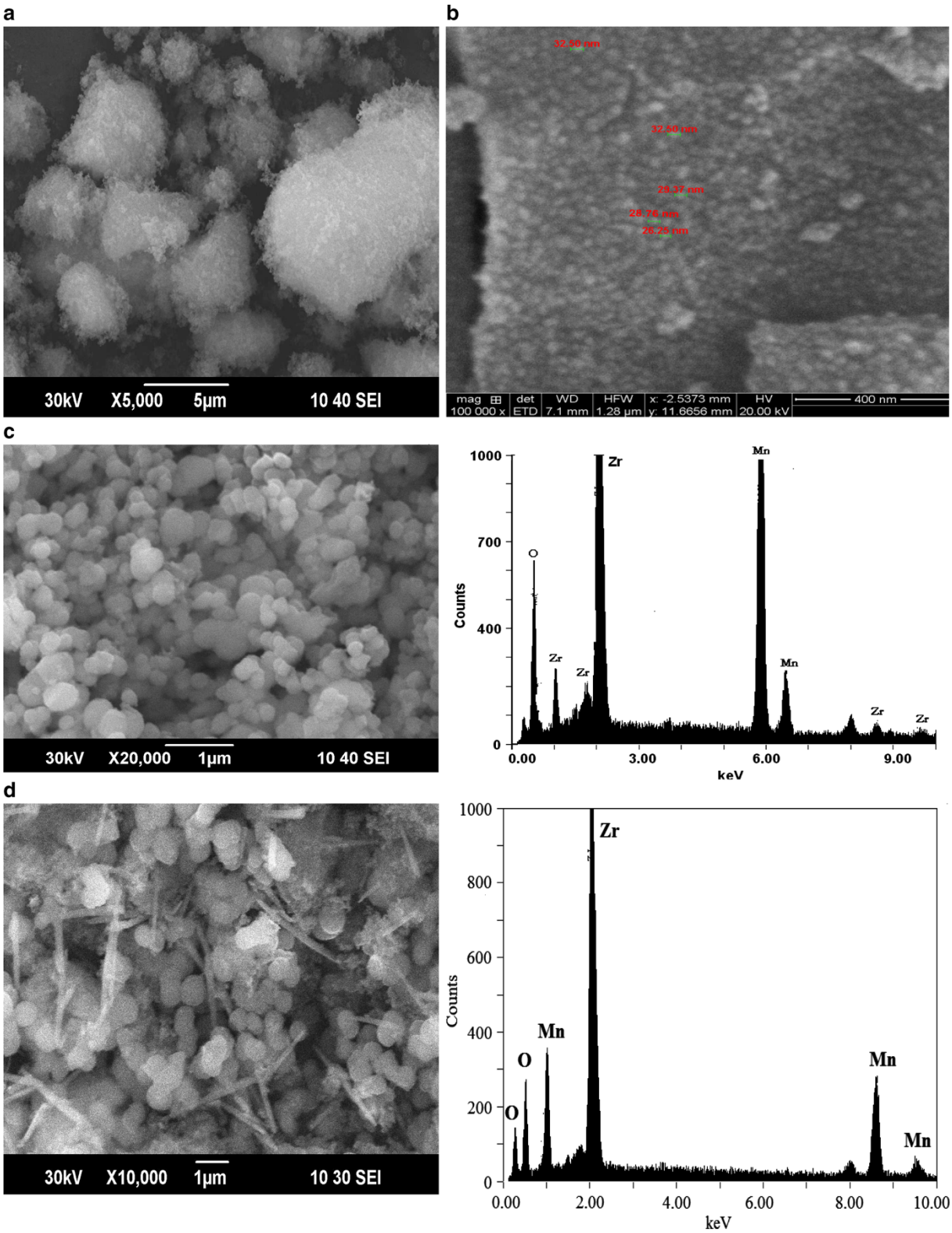

Fig. 3 SEM behavior of (**a**) nano MnO_2, **b** nano ZrO_2 and SEM image EDAX pattern of (**c**) MnO_2–ZrO_2, **d** MnO_2–ZrO_2, **e** MnO_2–ZrO_2, **f** MnO_2–ZrO_2, **g** 0.45 M MnO_2–ZrO_2

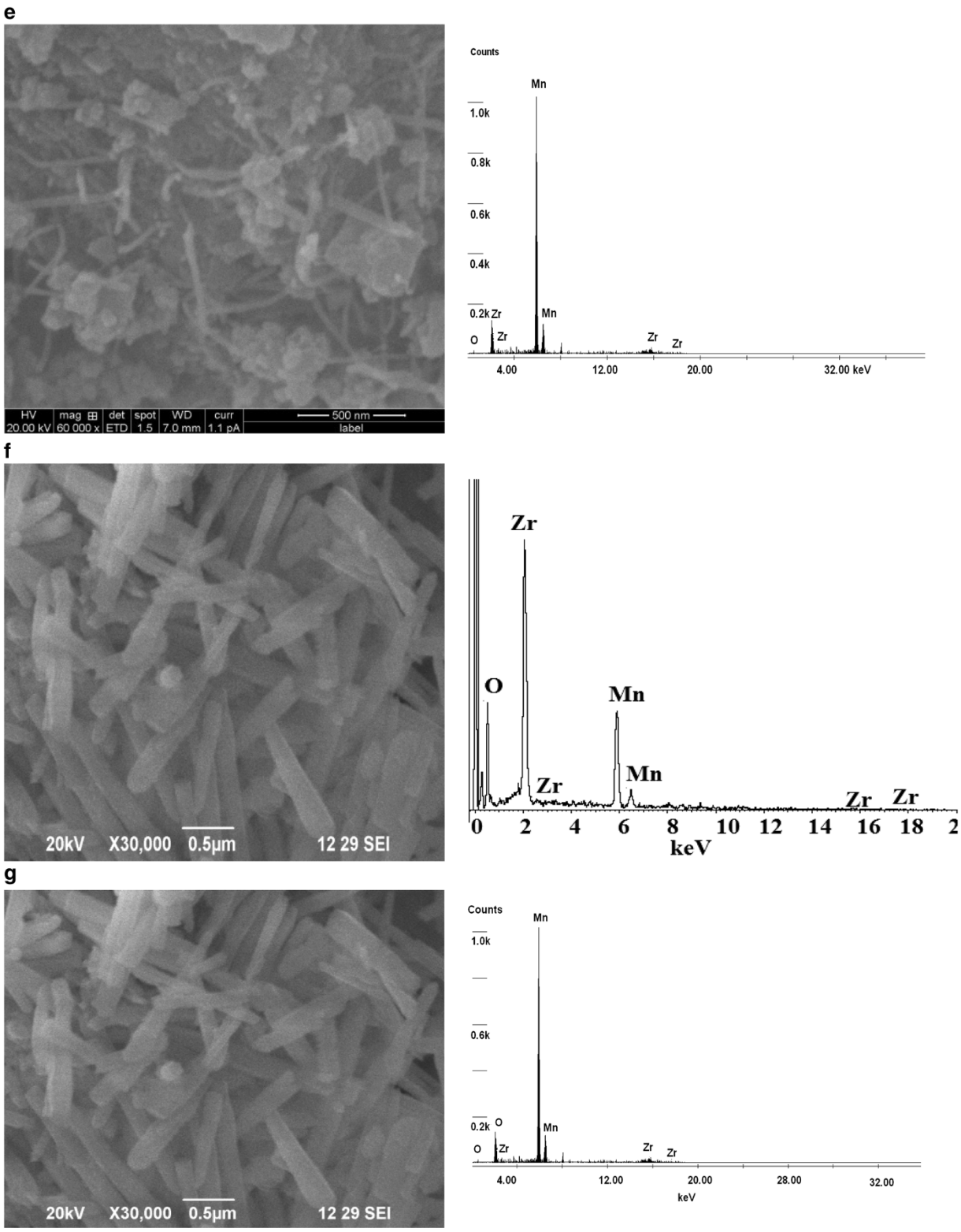

Fig. 3 continued

and $ZrOCl_2$ (0.05, 0.15, 0.25, 0.35, 0.45 M) is characterized by TGA/DTA analysis and the results are shown in Table 1. In these curves the first weight loss step from 42 to 170 °C corresponds to the loss of moisture. The next weight loss step from 91 to 390 °C corresponds to extra bounded water molecules. The final weight loss step from

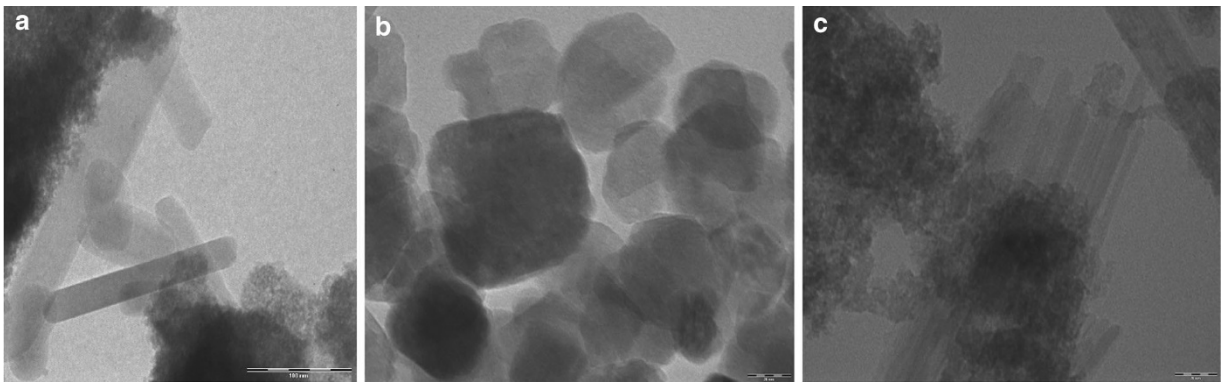

Fig. 4 TEM image of (**a**) nano ZrO_2, **b** MnO_2 nanoparticles, **c** MnO_2–ZrO_2 (0.45 M) nanorod

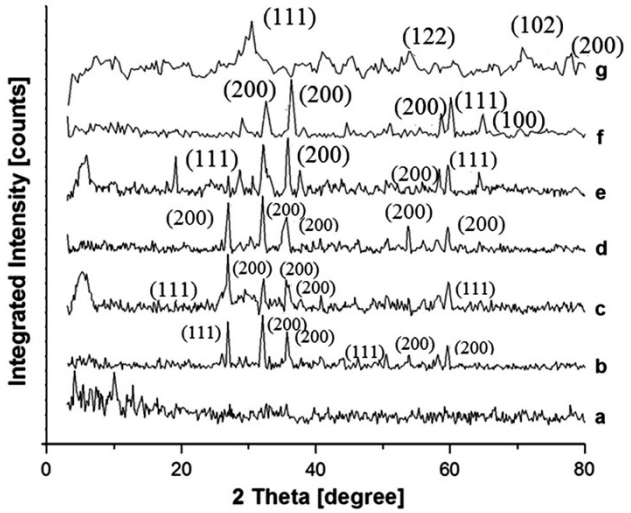

Fig. 5 XRD Pattern of (*a*) nano 0.05 M MnO_2–ZrO_2, (*b*) 0.15 M MnO_2–ZrO_2, (*c*) MnO_2–ZrO_2, (*d*) MnO_2–ZrO_2, (*e*) MnO_2–ZrO_2, (*f*) nano MnO_2, (*g*) nano ZrO_2

281 to 321 °C corresponds to the degradation of mixed oxides (MnO_2–ZrO_2). The weight loss values at the critical temperatures such as 280, 300, 320 and 390 °C reveal that the type of simple oxides employed affects the thermal properties of the resulting mixed oxides. The thermogram of 0.05 M MnO_2–ZrO_2 is shown in Fig. 6c.

DSC thermogram of MnO_2, ZrO_2 and different concentrations of mixed MnO_2–ZrO_2 are recorded at the heating rate 10 °C min^{-1}. The glass transition temperature (T_g) crystallization temperature (T_C) and melting point (T_M) of the mixed oxide are determined from the DSC curves (Fig. 7a) shows the melting point (T_M) of MnO_2 at a temperature of 237 °C and the (T_C) value at 220 °C. The melting point (T_M) of ZrO_2 was recorded at a temperature of 95 °C, the T_C value recorded at 10 °C and the T_g value recorded at −70 °C. These results can be seen in Fig. 7b. The T_C value of MnO_2–ZrO_2 mixed oxide is in the range of

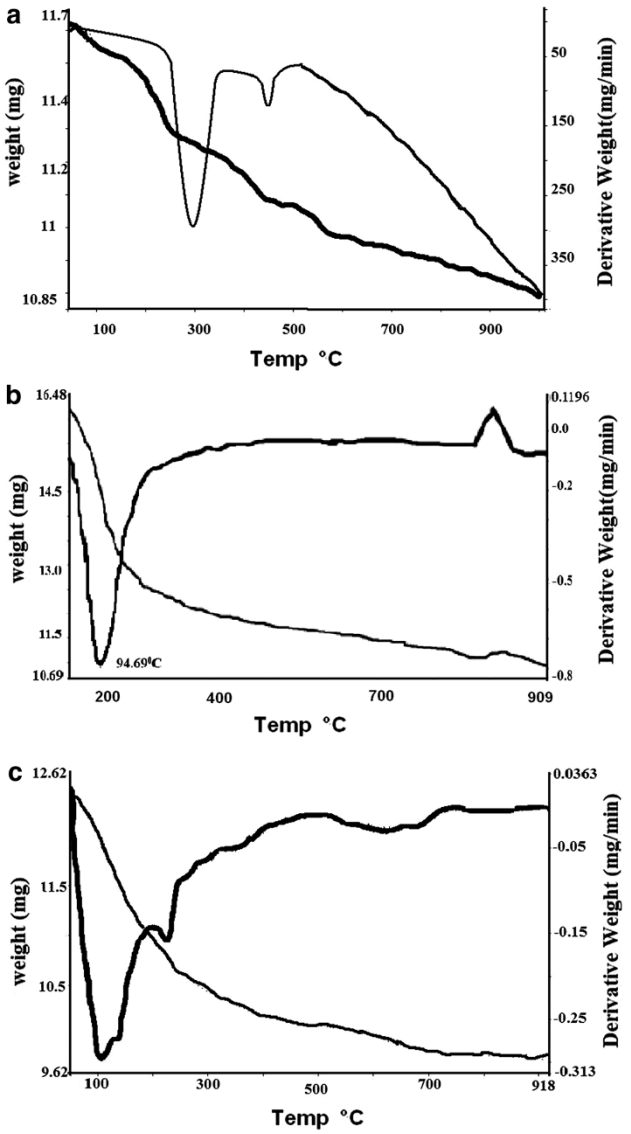

Fig. 6 TGA/DTA Curves of (**a**) nano MnO_2, **b** nano ZrO_2, **c** 0.05 M MnO_2–ZrO_2

Table 1 TGA analysis of nano ZrO_2, nano MnO_2 and MnO_2–ZrO_2 mixed oxides

Nanoparticles	Temperature due to loss of moisture (°C)	Temperature due to loss of water (°C)	Temperature due to degradation of mixed oxides (°C)
ZrO_2	30–100	101–170	From 171 onwards
MnO_2	42–90	91–580	From 581 onwards
0.05 M MnO_2–ZrO_2	55–170	171–390	From 391 onwards
0.15 M MnO_2–ZrO_2	42–100	101–320	From 321 onwards
0.25 M MnO_2–ZrO_2	45–180	181–320	From 321 onwards
0.35 M MnO_2–ZrO_2	42–90	91–300	From 301 onwards
0.45 M MnO_2–ZrO_2	45–120	121–280	From 281 onwards

29.93–36.35 °C. The mixed oxide was melted at the temperature range of 76.24–93.11 °C. According to DSC the melting temperature T_M of different concentrations of mixed oxide was decreased remarkably than the simple oxides. Table 2 shows the T_C and T_M values of 0.05–0.45 M MnO_2–ZrO_2 mixed oxides. DSC thermogram of 0.05 M MnO_2–ZrO_2 and is shown in Fig. 7c.

Cyclic voltammetric behavior of nano MnO_2, nano ZrO_2 and MnO_2–ZrO_2

Cyclic voltammetric studies of ZrO_2 exhibited one oxidation peak at 0.179 V with higher peak current at pH 1.0 which led to the selection of pH at 1.0 as optimum pH for further voltammetric studies. Cyclic voltammetric behavior of MnO_2 showed one anodic peak (Fig. 8a) at 0.415 V which is due to the presence of MnO_2 and it is reduced at 0.352 V. Cyclic voltammetric behavior of ZrO_2 showed one oxidation peak (Fig. 8b) observed at 0.179 V, which indicated the formation of ZrO_2, whereas for different concentrations of mixed oxides, two oxidation peaks were observed in the range 0.127–0.3238, 0.6,535–0.6571 V (Fig. 9), respectively, which were entirely different from the behavior, those obtained from nano MnO_2 and nano ZrO_2, confirmed the formation of mixed nano MnO_2–ZrO_2 oxide. Cyclic voltammetric behavior of nano MnO_2–ZrO_2 mixed oxides synthesized at five different concentrations of both $MnSO_4$ and $ZrOCl_2$ (0.05, 0.15, 0.25, 0.35, 0.45 M) are shown in Fig. 9a–e. With the increase in concentrations (0.05–0.45 M) of nano MnO_2–ZrO_2

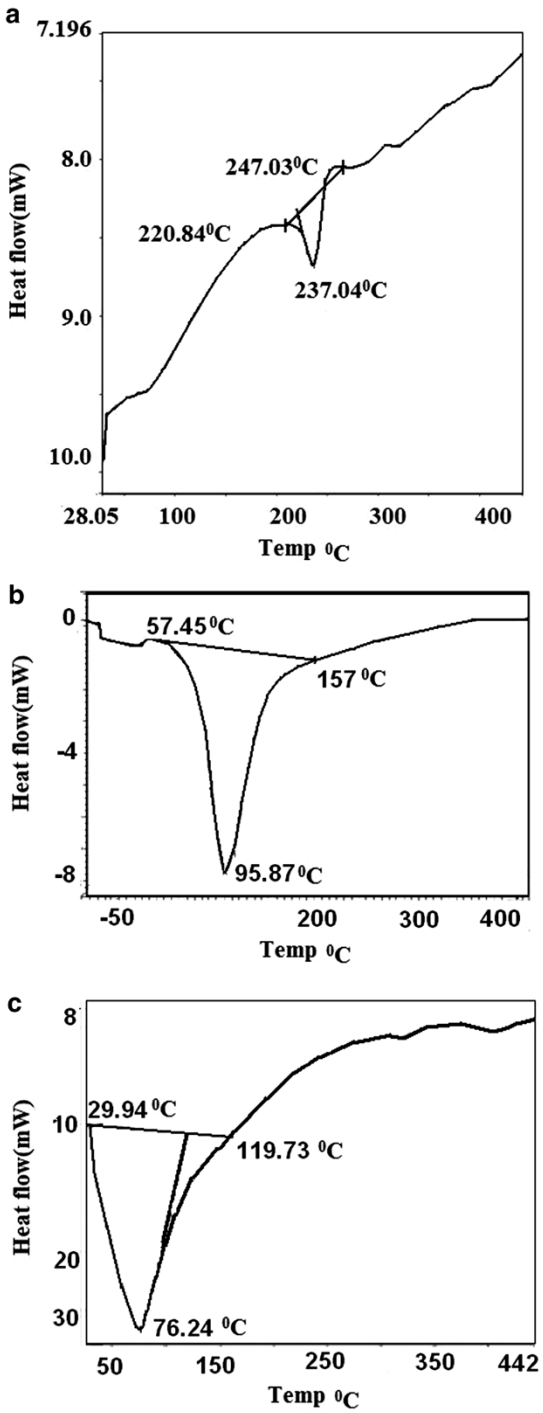

Fig. 7 DSC Thermograms of (**a**) nano MnO_2, **b** nano ZrO_2, **c** 0.05 M MnO_2–ZrO_2

there is corresponding increase in peak potentials and peak currents also.

The plot of peak current versus different scan rate for nano MnO_2–ZrO_2 mixed oxide exhibits a straight line (Fig. 10) indicating a good adherent behavior on electrode surface. When peak currents of nano MnO_2–ZrO_2 are correlated with the square root of scan rate, a straight line is

Table 2 T_C and T_M for 0.05–0.45 M MnO_2–ZrO_2 mixed oxides

Concentration of MnO_2–ZrO_2 nanoparticles (M)	T_C °C	T_M °C
0.05	29.94	76.24
0.15	36.35	77.20
0.25	32.60	81.90
0.35	29.93	82.41
0.45	34.59	93.11

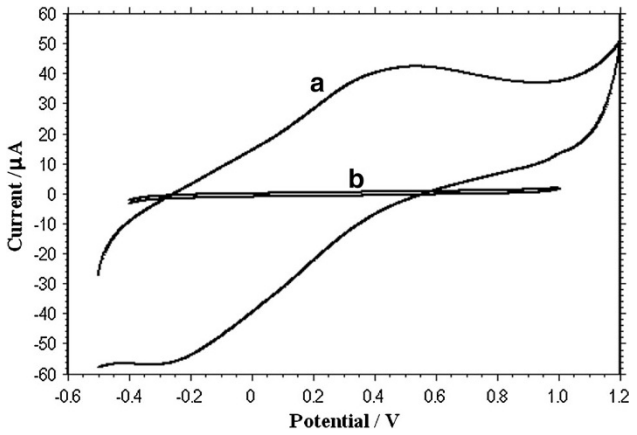

Fig. 8 Cyclic Voltammetric behavior of (a) nano MnO_2, b nano ZrO_2

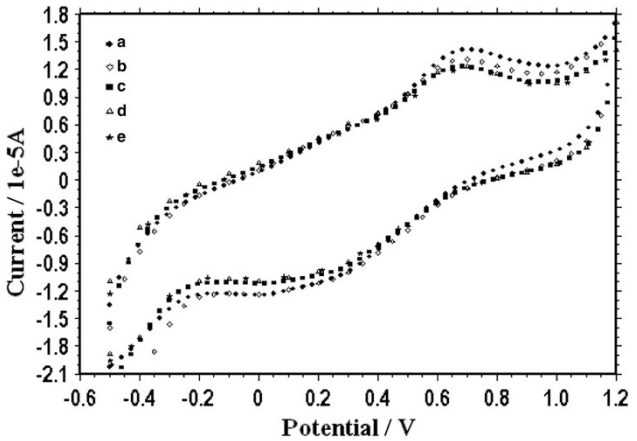

Fig. 9 Cyclic voltammetric behavior of (a) 0.05 M nano MnO_2–ZrO_2, b 0.15 M MnO_2–ZrO_2, c 0.25 M MnO_2–ZrO_2, d 0.35 M MnO_2–ZrO_2, e 0.45 M MnO_2–ZrO_2

observed (Fig. 11). These facts reveal that the voltammetric redox behavior of mixed metal oxide nanoparticles is controlled by adsorption process. Thus it proves to be an anticorrosive agent for paints.

When the metal salts of Mn and Zr were mixed during chemical co-precipitation, the mixed metal oxide nanoparticles were produced. The mixed metal oxide was coated on glassy carbon electrode and the cyclic voltammogram was recorded. The voltammogram also exhibited oxidation and reduction peaks with higher peak current.

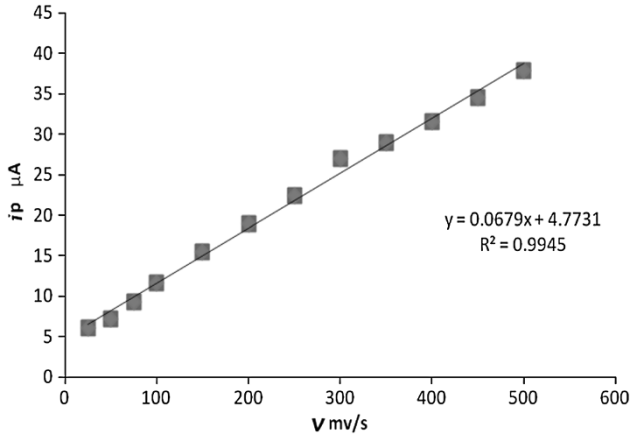

Fig. 10 Plot of peak current versus scan rate for 0.45 M nano MnO_2–ZrO_2

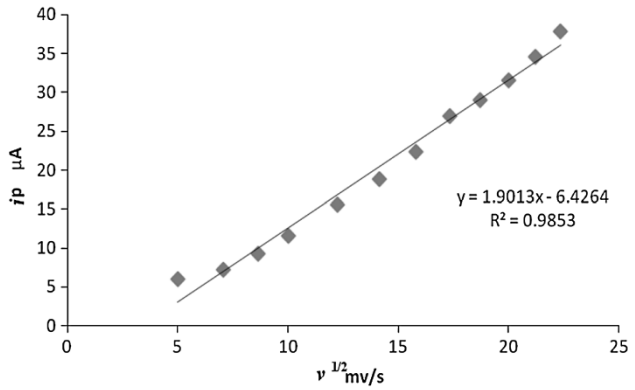

Fig. 11 Plot of peak current versus square root of scan rate for 0.45 M nano MnO_2–ZrO_2

This might be due to the formation of mixed oxide from metal salts of Mn and Zr.

The increase in the peak current of the mixed oxide from that of simple oxides and the increase in the peak current due to increase in the metal concentration confirm the increase in the conductivity of the mixed oxide. To temper the cutting edge of electrochemistry, it will be necessary to carry out capacitance measurements, as these are closer to bulk-like techniques.

For a simple parallel plate capacitor, charge on the capacitor, Q, is proportional to the voltage drop across the capacitor V, and C is the capacitance. Therefore the equation is

$$Q = CV$$

Capacitance is a crucial factor in electrochemical experiments because it gives rise to current during the charging of the capacitor. To calculate the magnitude of this current, with respect to time (t) and capacitance should be treated as constant recognizing that dQ/dt is an expression for current and dV/dt is the potential scan rate. The equation is

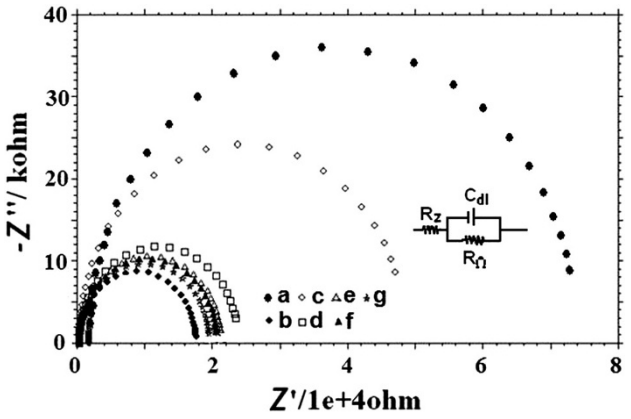

Fig. 12 Electrochemical impedance spectra of (a) nano MnO_2, b nano ZrO_2, c 0.05 M MnO_2–ZrO_2, d 0.15 M MnO_2–ZrO_2, e 0.25 M MnO_2–ZrO_2, f 0.35 M MnO_2–ZrO_2, g 0.45 M MnO_2–ZrO_2

$$dQ/dT = C dV/dt$$

Therefore $i = Cv$

From this very simple derivation, we have an expression for the charging current at the steady state when applying a ramping voltage. If there are no possibilities for electron transfer between the solution and the electrode this is the only current that we will observe. The cyclic voltammogram of mixed oxide shows the influence of various scan rates. The capacitance was calculated from cyclic voltammograms using the above said equation. The calculated values of MnO_2, ZrO_2 and 0.05 M MnO_2–ZrO_2 mixed oxide are 13, 30 and 39 μF respectively. The capacitance of chemically synthesized mixed oxide is suggested that, they can well be used as an electronic material.

EIS studies of nano MnO_2, nano ZrO_2 and MnO_2–ZrO_2

Electrochemical impedance measurements were carried out at a frequency range say from 1,000 to 0.01 Hz at open circuit potential. The simple equivalent Randle circuit for studies is given as an insert in (Fig. 12). The chemically synthesized simple oxide and mixed oxide nanoparticles coated on glassy carbon electrode are used (0.0314 cm^2) as working electrode. The cell is composed by a 1.0 cm^2 Pt electrode, Ag/AgCl serves as reference electrode. The measurements were made for simple oxides such as nano MnO_2, nano ZrO_2 (Fig. 12a, b) and nano MnO_2–ZrO_2 mixed oxides synthesized at five different concentrations of both $MnSO_4$ and $ZrOCl_2$ (0.05, 0.15, 0.25, 0.35, 0.45 M) as shown in Fig. 12c–g. To understand the electrical properties of the electrode/interfaces clearly the Randle's equivalent circuit was chosen to fit the obtained impedance data. In Randle's circuit, it is assumed that the resistance to charge transfer (R_{ct}) and the diffusion impedance (R_{ct}) are parallel to the interfacial capacity (C_{dl}). The parallel combination of R_{ct} and C_{dl} gives rise to a semicircle in the complex plane plot of Z'' against Z', the semicircle diameter equals charge transfer resistance (R_{ct}). This resistance exhibits the electron transfer kinetics of the redox probe at the electrode interface. From the Table 3, it is clear that the decrease in electrical resistivity with the increase in concentration is due to the improvement in crystallite and/or grain size, decrease in defects. This fact confirms the anticorrosive activity of the synthesized nano MnO_2–ZrO_2 mixed oxide samples. The lower the concentration of MnO_2–ZrO_2 mixed oxide nanoparticles, higher the resistance which is responsible for anti corrosive activity. The small observed variations might be from the nature of electrode conductivities (Chandrasekaran et al. 2008). More resistivity implies a physical adsorption of the corresponding electrodes during the diffusion path way whereas the lower value indicates the good conductivity behavior.

Table 3 R_{ct} and C_{dl} for 0.05–0.45 M MnO_2–ZrO_2 mixed oxides

Concentration of nano MnO_2–ZrO_2 M	R_{ct} (Ω cm^2)	C_{dl} (μF cm^{-2})
0.05	8.393	0.0107
0.15	2.353	0.0769
0.25	2.113	0.1000
0.35	2.053	0.1053
0.45	1.940	0.1205

Conclusion

To summarize, nano MnO_2, ZrO_2 and MnO_2–ZrO_2 were synthesized by wet chemical method. The characterizations of the chemically synthesized nanoparticles were done using UV–Visible spectroscopic and FTIR studies. The sizes of the synthesized oxides were in the nm range and they were found to be thermally stable. SEM and TEM studies show a uniform rod-like morphology in the case of mixed oxide. CV studies revealed that the mixed oxide has good adherent and electrochemical activity on GC and thus it is found to be corrosive protection agent for paints formulation. The capacitance of chemically synthesized mixed oxide was suggested that, they might well be used as an electronic material.

Acknowledgments The authors are extremely grateful to Department of Science and Technology (FAST TRACK and FIST) New Delhi, INDIA for using CHI Electrochemical workstation at V.O.C.College, Tuticorin-8 and Jasco UV–VISIBLE Spectrophotometer.

References

Brock SL, Duan NG, Tian ZR, Giraldo O, Zhou H, Suib SL (1998) A review of porous manganese oxide materials. Chem Mater 10:2619–2628

Chandrasekaran R, Soneda Y, Yamashita J, Kodama M, Hatori H (2008) Effect of poly(3,4-ethylenedioxythiophene) (PEDOT) in carbon-based composite electrodes for electrochemical supercapacitors. J Solid State Electrochem 12:1349–1352

Chen Y, Liu C, Li F, Chen H-M (2005) Preparation of single-crystal α-MnO_2 nanorods and nanoneedles from aqueous solution. J Alloy Compd 397:282–285

Dietl T, Matsukura H, Cibert F, Ferrand J, Zener D (2000) Model description of ferromagnetism in zinc-blende magnetic semiconductors. Science 287:1019–1022

Dong X, Zhang X, Liu B, Wang H, Li Y, Huang Y, Du Z (2006) Synthesis of manganese oxohydroxide (MnOOH) and Mn_3O_4 Nanorods using novel reverse micelles. J Nanosci Nanotechnol 6:818–822

Du F, Liu J, Guo Z, Shape J (2009) Controlled synthesis of CuO and its catalytic application to synthesise amorphous carbon nanofibres. J Mater Res Bull 44:25–29

Feng Q, Kanoh H, Ooi K (1999) Manganese oxide porous crystals. J Mater Chem 9:319–333

Guedes M, Ferreira JMF, Ferro AC (2009) Dispersion of CuO particles in aqueous suspensions containing 4,5-dihydroxy 1,3-benzenedisulphonic acid disodium salt. J Ceram Int 35:1939–1945

Hosono E, Kudo T, Honma I, Matsuda H, Zhou HS (2009) Synthesis of single crystalline spinel $LiMn_2O_4$ nanowires for a lithium ion battery with high power density. Nano Lett 9:1045–1051

Lu W, Lieber CM (2006) Semiconductor nanowires. J Phys D Appl Phys 39:R387–R406

Luo X-L, Xu J-J, Zhao W, Chen H-Y (2004) Cholesterol biosensor based on MWCNTs-MnO_2 Nanoparticle using FFT continuous cyclic voltammetry. Biosens Bioselectron 19:1295–1300

Partha Sarathi V, Thilagavathi G (2011) Synthesis and characterization of zinc oxide nanopartilce and its application on fabrics for microbe resistant defence clothing. Int J Pharm Pharm Sci 3:392–398

Perez-Maquedaa LA, Matijevicb E (1997) Preparation and characterization of nanosized zirconium (hydrous) oxide particles. J Mater Res 12:3286–3292

Rema Devi BS, Raveendren R, Vaidyan AV (2007) Synthesis and characterization of Mn^{2+}-doped ZnS nanoparticles. Pramana J Phys 68:679–687

Shi R, Wang YJ, Li D, Xu J, Zhu YF (2010) Synthesis of $ZnWO_4$ nanorods with [100] orientation and enhanced photocatalytic properties. Appl Catal B Environ 100:173–178

Singh DK, Pandey DK, Yadav RR, Singh D (2012) A study of nanosized zinc oxide and its nanofluid. Pramana J Phys 78:759–766

Subramanian V, Zhu H, Wei B (2008) Nanostructured manganese oxides and their composites with carbon nanotubes as electrode materials for energy storage devices. Pure Appl Chem 80:2327–2343

Wambach J, Baiker A, Wokaun A (1999) CO_2 hydrogenation over metal/zirconia catalysts. Phys Chem Chem Phys 1:5071–5080

Wang ZL (2000) Characterizing the structure and properties of individual wire like nano entities. Adv Mater 12:1295–1298

Xia YN, Yang PD, Sun YG, Wu XY, Mayers B, Gates B, Yin YD, Kim F, Yan HQ (2003) One-dimensional nanostructures: synthesis, characterization and applications. Adv Mater 15:353–389

Yang H, Zhu S, Pan N (2004) Studying the mechanisms of titanium dioxide as ultraviolet-blocking additive for films and fabrics by an improved scheme. J Appl Polym Sci 92:3201–3210

Yu KH, Chen JH (2009) Enhancing solar cell efficiencies through 1-D nanostructures. Nanoscale Res Lett 4:1–10